DOI: 10.1002/cphc.200900914

Tailored Porous Silicon Microparticles: Fabrication and Properties

Ciro Chiappini,[b] Ennio Tasciotti,[a] Jean R. Fakhoury,[a] Daniel Fine,[a] Lee Pullan,[c] Young-Chung Wang,[c] Lianfeng Fu,[c] Xuewu Liu,*[a] and Mauro Ferrari*[a]

The use of mesoporous silicon particles for drug delivery has been widely explored thanks to their biodegradability and biocompatibility. The ability to tailor the physicochemical properties of porous silicon at the micro- and nanoscale confers versatility to this material. A method for the fabrication of highly reproducible, monodisperse, mesoporous silicon particles with controlled physical characteristics through electrochemical etching of patterned silicon trenches is presented. The particle size is tailored in the micrometer range and pore size in the nanometer range, the shape from tubular to discoidal to hemispherical, and the porosity from 46 to over 80%. In addition, the properties of the porous matrix are correlated with the loading of model nanoparticles (quantum dots) and their three-dimensional arrangement within the matrix is observed by transmission electron microscopy tomography. The methods developed in this study provide effective means to fabricate mesoporous silicon particles according to the principles of rational design for therapeutic vectors and to characterize the distribution of nanoparticles within the porous matrix.

Introduction

Exploratory work demonstrating porous silicon biodegradability[1,2] and biocompatibility[3–7] opened the avenue for its use in implantable devices,[8] drug-delivery systems,[9,10] and scaffolds for tissue engineering.[11,12] Porous silicon particles (PSPs) have been shown to tune drug solubility,[10] increase bioavailability,[13] and enable sustained release.[9] Our group recently presented a multistage drug-delivery system (MDS) based on PSPs.[9,14,15] The prototypical MDS consists of different types of therapeutic and diagnostic second-stage nanoparticles (NPs; liposomes, dendrimers, quantum dots, gold nanoshells, etc.) loaded into the pores of an optimally engineered first-stage PSP. The use of PSPs in the MDS provides the ability to simultaneously carry, protect, and release in a controlled fashion a variety of NPs with very different features and functions.

In the last two decades, a vast assortment of NPs has been developed for both therapeutic intervention and imaging.[16–18] They differ significantly in terms of size, composition, and structure, and the loading of NPs within the pores of the PSP strictly depends on their relative physicochemical compatibility. Consequently, an efficient MDS requires first-stage PSP carriers with variable porous structures capable of hosting and retaining a multitude of different second-stage NPs. Furthermore, the interaction of the MDS with target cells[19] and the rates and mechanisms of cellular internalization[15,20] are strongly influenced by the size and shape of the PSPs. Similarly, the ability of the PSPs to navigate the vasculature proficiently, as dictated by their margination characteristics, depends on their size, geometry, and aspect ratio.[21] Finally, the pharmacokinetics of the therapeutic payload can be linked to the biodegradation rates of the PSPs, which are determined by their pore size and porosity.[9,22]

Although some results have been achieved in patterning porous silicon layers into particles,[23,24] the necessary control of the features at the micro- and nanoscale was not yet satisfactory. The current standard technique for the fabrication of PSPs consists of sonication or ball milling of porous silicon layers, which results in polydisperse fragments of random size and shape.[10,25,26] Herein, we present a microfabrication technique that enables the fine tailoring of monodisperse PSPs at the submicrometer scale. The technique we describe provides precise control over the key parameters necessary to tune the interaction of PSPs with both biological systems and nanoparticulates: size, shape, and aspect ratio, as well as porosity, pore size, and pore morphology. We furthermore demonstrate the use of this system as a carrier for NPs and describe their loading inside the pores by direct visualization through electron microscopy.

[a] Dr. E. Tasciotti, J. R. Fakhoury, Dr. D. Fine, Dr. X. Liu, Dr. M. Ferrari
Department of Nanomedicine and Biomedical Engineering
The University of Texas Health Science Center at Houston
Houston, TX 77030 (USA)
Fax: (+1) 713 500 2462
E-mail: xuewu.liu@uth.tmc.edu
mauro.ferrari@uth.tmc.edu

[b] C. Chiappini
Department of Biomedical Engineering
The University of Texas at Austin, Austin, TX 78712 (USA)

[c] Dr. L. Pullan, Y.-C. Wang, L. Fu
FEI Company, Hillsboro, OR 97124 (USA)

Supporting information for this article is available on the WWW under http://dx.doi.org/10.1002/cphc.200900914.

Results and Discussion

A 100 mm p++ silicon wafer was patterned by photolithography and etched through a silicon nitride sacrificial layer (Figure 1a). The pattern was transferred into the silicon layer by various etch methodologies, to determine different shapes of the trench that nucleated PSPs with different profiles (Figure 1b). Subsequently, an electrochemical etch process formed PSPs of desired porosity, pore size, and thickness. Following PSP formation, a high current density was applied to create a highly porous layer at the PSP/wafer interface (release layer; Figure 1c). The silicon nitride layer was removed in HF (Figure 1d) and the PSPs were released from the substrate, suspended in isopropanol (IPA), and preserved at 20 °C in a controlled-temperature environment.

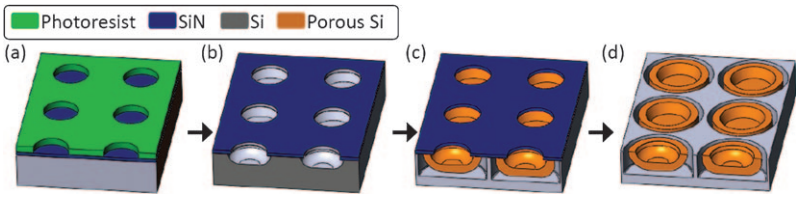

Figure 1. Schematic depiction of the fabrication process. a) Pattern transfer to the photoresist layer on top of the sacrificial SiN layer. b) Trench formation in the Si substrate through a combination of dry and wet etching. c) Formation of the PSPs and release layer following anodic etching. d) PSPs ready to be released by ultrasonication in IPA following stripping of the SiN mask.

This method, which is further described in the Experimental Section, allowed for the microfabrication of a variety of well-controlled and reproducible PSPs (Figures 2 and 3). The shape of the PSPs was determined by the unit shape on the photolithographic mask employed, as the nucleation site retained the exact shape of the lithographic pattern. The shape of the electrochemical etch undercut, which constituted the external corona, was determined by the current distribution between the nearest-neighbor PSPs and was independent of the profile of the trench. Statistical analysis of the scanning electron microscopy (SEM) images of 160 PSPs from independently produced lots confirmed the accuracy and reproducibility of the process. The analysis showed that PSPs with a circular nucleation site 2 ± 0.1, 1 ± 0.1, or 0.67 ± 0.08 μm in diameter surrounded by a rounded square external corona with an edge length of 3.2 ± 0.1, 1.6 ± 0.1, or 0.97 ± 0.08 μm, respectively, originated from 2, 1, or 0.6 μm circular lithographic patterns (Figures 3a,b). The thickness of the electrochemical etch undercut constituting the external corona was 600, 300, or 150 nm for the 2, 1, or 0.6 μm patterns, respectively. The nucleation site circularity was 0.98 ± 0.05 and the ratio of the particle's width to its length was 0.98 ± 0.06. The PSP profile was determined by the nucleation trench formed in the silicon prior to its porosification.

SEM image analysis of 3.2 μm PSPs showed that wet etching of the masking layer yielded flat-disk PSPs (Figures 3c,d); a 4 min CF_4 etch formed a 180 nm trench in the silicon that yielded discoidal PSPs (Figures 3e,f); a 4 min SF_6 etch formed a 475 nm quasi-isotropic trench that yielded hemispherical PSPs (Figures 3g,h); a 6 min HBr etch followed by a 1 min SF_6 etch formed a 975 nm anisotropic trench that yielded tubular PSPs (Figures 3i,j). The combination and timing of different etch procedures allowed tight control over the final shape and aspect ratio of the PSPs. The undercut for the different shapes was maintained at 600 nm to guarantee a uniform PSP size of 3.2 μm. The resulting thickness of the porous layer at the bottom of the trench was 605 nm for wet etching, 795 nm for CF_4 etching, 720 nm for SF_6 etching, and 780 nm for $HBr+SF_6$ etching, thus showing a slight dependence of the electrochemical etch isotropy on the trench morphology. The PSP aspect ratio was tuned from 1.8 for tubular PSPs to 5.3 for flat PSPs.

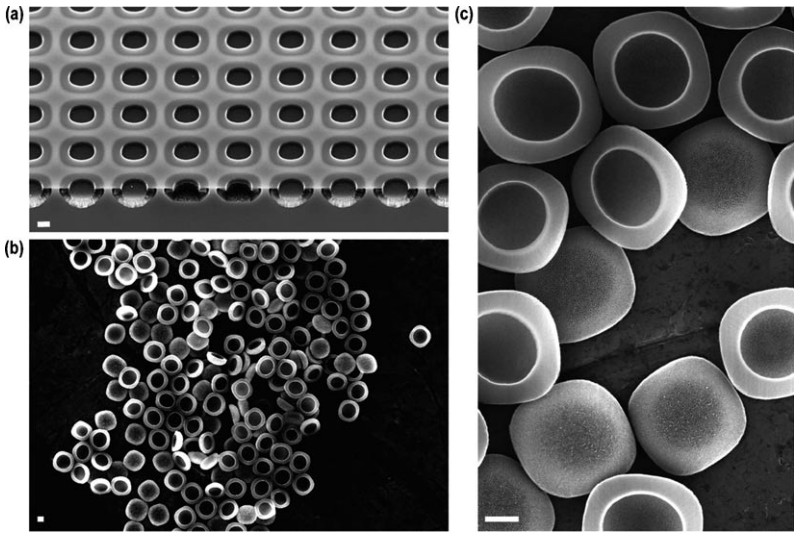

Figure 2. SEM images of large clusters of PSPs. The PSPs are characterized by size and shape uniformity. a) HBr_6-etched tube-shaped MP3 PSPs still attached to the silicon substrate before the removal of the silicon nitride sacrificial layer and the PSPs' subsequent release. b) Overview of a large cluster of SF_6-etched bowl-shaped MP3 PSPs following release by sonication in IPA. c) Close-up of a small cluster of CF_4-etched discoid-shaped MP3 PSPs following release by sonication in IPA. All scale bars: 1 μm. MP3 = medium-pore sample.

Different PSP types were characterized by N_2 desorption isotherms to evaluate their porosity and pore size distribution. The PSPs used for this analysis origi-

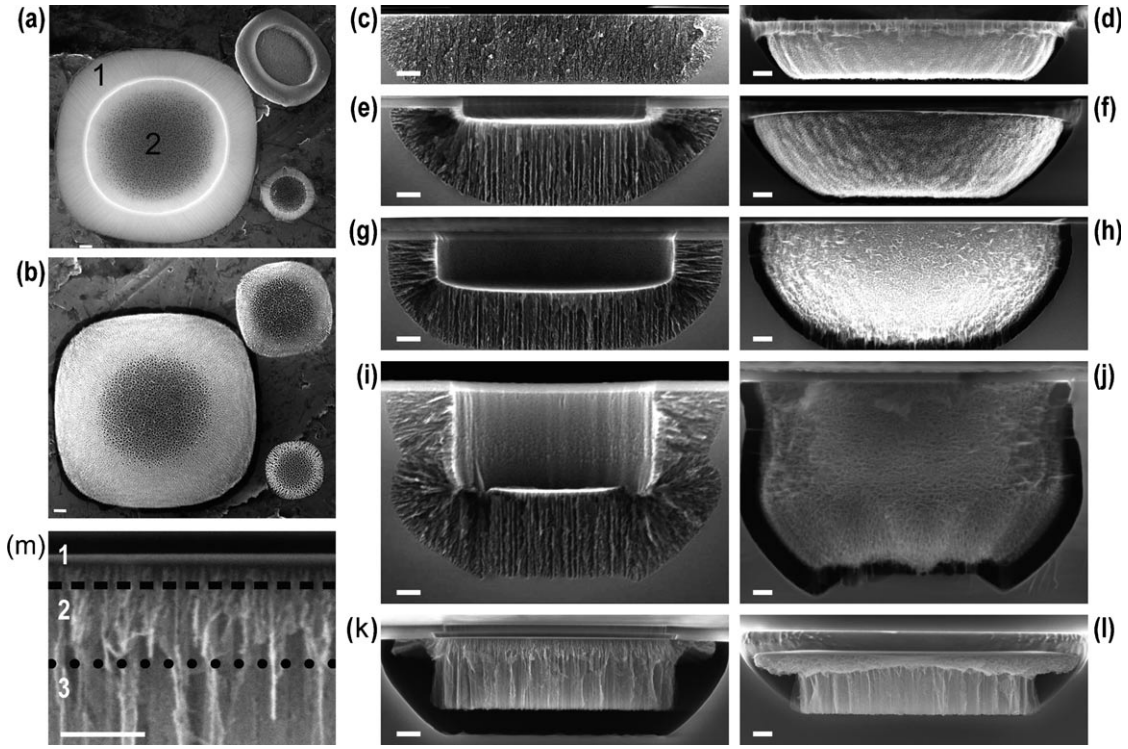

Figure 3. SEM images of PSPs. a) Digital composition of three distinct micrographs showing the nucleation side of 3.2, 1.6, and 0.97 μm PSPs: 1) the external corona and 2) the nucleation site. b) Digital composition of three distinct micrographs showing the release side of 3.2, 1.6, and 0.97 μm PSPs. Section along the diameter and the lateral view of: a flat-disk PSP obtained by wet etching of the masking layer (c, d, respectively); a discoidal PSP obtained by trench formation by CF_4 reactive-ion etching (RIE; e, f, respectively); a hemispherical PSP obtained by trench formation by SF_6 RIE (g, h, respectively); a tubular PSP obtained by trench formation by a combination of HBr and SF_6 RIE (i, j, respectively); and an XLP1 PSP (k, l, respectively). m) Close-up view of the multilayer structure of an XLP1 particle: 1) SP layer, 2) transitional layer, 3) XLP layer. c–m) The nucleation side is at the top and the release side at the bottom. All scale bars: 200 nm.

nated from independent production lots. The analysis proved that each of the specific pore sizes could be consistently reproduced, as demonstrated by the absence of multiple peaks in the pore distribution curves. Figure 4 summarizes the Barrett–Joyner–Halenda (BJH) model analysis of the desorption curves. The average pore size ranged from (5.9 ± 2.1) nm (small-pore PSPs: SPs) to (51.3 ± 28.7) nm and larger (extra-large-pore PSPs: XLPs) depending on the porosification conditions (Figure 4b). PSPs with pore sizes of (10.1 ± 3.9), (15.2 ± 6.3), and (17.9 ± 6.5) nm (medium-pore PSPs: MPs) as well as PSPs with pore sizes of (20.9 ± 7.9) and (26.3 ± 14.6) nm (large-pore PSPs: LPs) were also obtained, thus demonstrating the ability to finely control pore size in a PSP (Figures 4b–d). As previously reported in the literature,[27] the standard deviation increased for larger-pore PSPs.

Porosity was positively correlated with pore size and ranged from 47.5% for SPs to 82.0% for XLP1. Intermediate values were 46.3, 51.1, 52.7, 55.7, and 66.1% for MP1, MP2, MP3, LP1, and LP2, respectively (Figures 4b–d). Evaluation of the porosity and pore size of XLP1 PSPs was underestimated since the BJH model applies only to the 3–50 nm range[27] (Figure 4c). The XLP2 pore size and porosity could not be measured by N_2 isotherms and were instead characterized by SEM. Pore morphology varied from randomly oriented, densely branched pores for SPs to structures with short branches for MPs to smooth parallel pores for LPs and larger pores (Figure 4a), as reported in the literature.[28] We also demonstrated the ability to combine multiple porous layers with different pore sizes in a single PSP. This multilayered structure was crucial to provide the mechanical stability needed to fabricate the XLPs. XLPs were produced through a continuous electrochemical etch process by means of a time-varying etch current. The initial SP stabilization layer (approximately 20 nm thick) was followed by a transitional layer from SP to XLP (approximately 70 nm thick); these two layers guaranteed the structural integrity of the PSP. The XLP layer of desired thickness and pore size was then formed at the bottom of the transitional layer (Figures 3k–m).

We furthermore exploited the positioning of an SP layer within a multilayer PSP structure to obtain functionally different porous structures. During the standard electrochemical etch, a thin layer of nanopores (nucleation layer) was formed in the initial phase of the etch due to transient currents, effectively capping the pores on the nucleation site. The capping nucleation layer was removed by means of a short CF_4 etch following the electrochemical process to expose the underlying porous structure and obtain PSPs with pass-through pores of constant diameter (Figure 5). Inverted PSPs with the nucleation layer removed and a capping layer on the opposite side were obtained by combining the short CF_4 etch with a two-layer PSP structure terminated by an SP layer. The three alternative

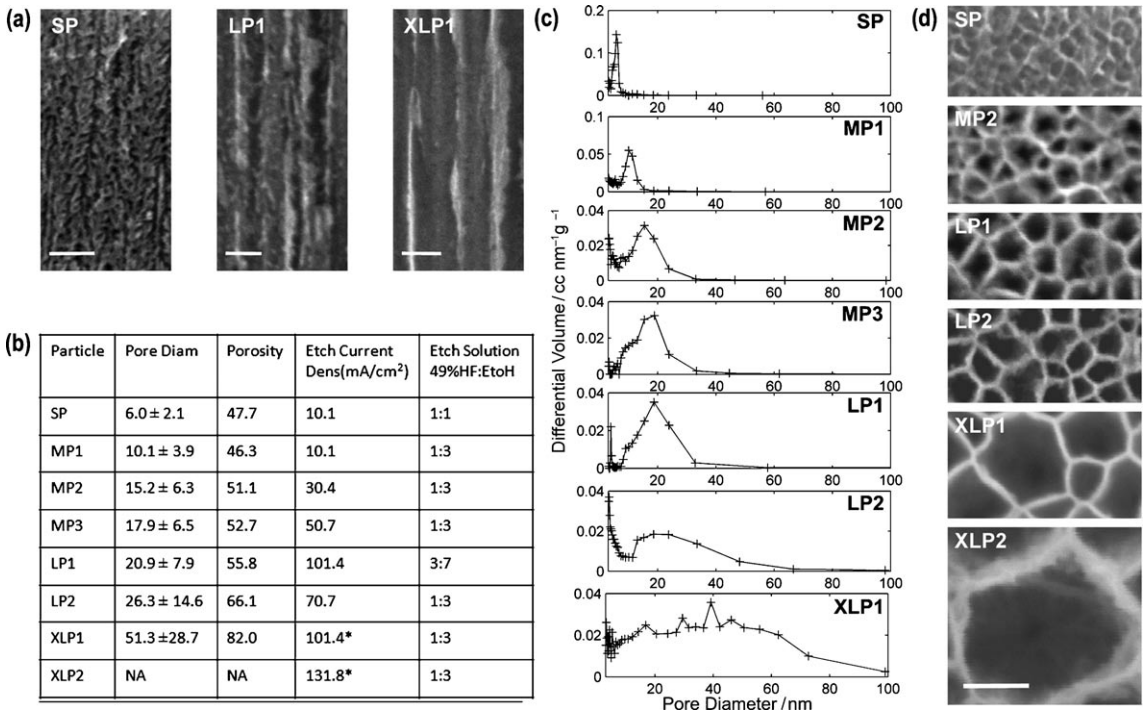

(b)

Particle	Pore Diam	Porosity	Etch Current Dens(mA/cm^2)	Etch Solution 49%HF:EtoH
SP	6.0 ± 2.1	47.7	10.1	1:1
MP1	10.1 ± 3.9	46.3	10.1	1:3
MP2	15.2 ± 6.3	51.1	30.4	1:3
MP3	17.9 ± 6.5	52.7	50.7	1:3
LP1	20.9 ± 7.9	55.8	101.4	3:7
LP2	26.3 ± 14.6	66.1	70.7	1:3
XLP1	51.3 ±28.7	82.0	101.4*	1:3
XLP2	NA	NA	131.8*	1:3

Figure 4. Analysis of the porous structure of the PSPs. a) SEM images of the PSP porous structure cross section along the pore axis, perpendicular to the Si(100) surface for the most representative pore structures investigated. b) Summary of the BJH analysis and the electrochemical etch parameters employed in the porosification of the PSPs. The etch current density reported for XLPs refers to the XLP layer. c) BJH model estimate of the differential volume of pores in the 3 to 100 nm range for all the different types of PSPs investigated. BJH analysis of XLP2 PSPs is not shown due to the inadequacy of the model. d) SEM images of the central bottom region of the PSP for the most representative pore sizes investigated (all scale bars: 100 nm).

porous structures obtained (opening on rear side, pass through, opening on front side) allow control of the direction of the loading of NPs within the porous matrix and their subsequent release.

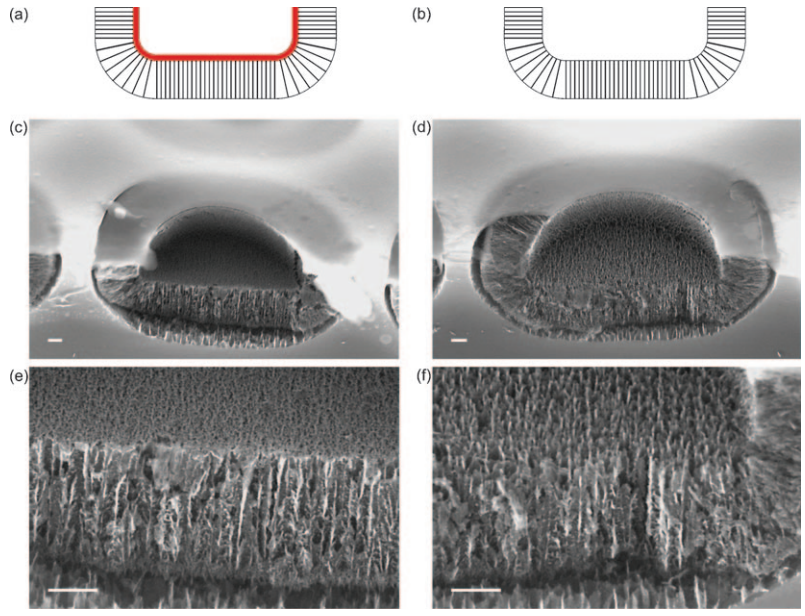

Figure 5. A short CF_4 plasma etch following the formation of the PSP results in the removal of the nucleation layer and formation of pass-through pores. a) Schematic depiction of a PSP as anodically etched; the small-pore nucleation layer is indicated in red. b) Schematic depiction of a PSP following a 15 s CF_4 plasma etch. c–f) 45° tilt SEM cross sections of a PSP with (c,e) and without (d,f) a nucleation layer. No damage to the PSP or the remaining pore structure due to the plasma etch is observed. All scale bars: 200 nm.

To demonstrate the key role of pore size and morphology in the control of the loading of NPs within the porous silicon matrix, we mixed carboxyl-terminated quantum dots (Q-dots) with different PSPs functionalized with 3-aminopropyltriethoxysilane (APTES) to obtain an amine-terminated surface. After optimization of the loading protocols,[9] we generated cross sections of the PSPs and analyzed them by high-angle annular dark-field scanning transmission electron microscopy (HAADF-STEM) coupled with mapping energy-dispersive X-ray (EDX) spectroscopy. Figure 6 shows how differently the Q-dots diffused within the pores or adhered on the surface of the PSPs as a function of pore size. HAADF-STEM imaging showed surface-functionalized CdSe Q-dots (15 nm hydrodynamic diameter, 5 nm metal core

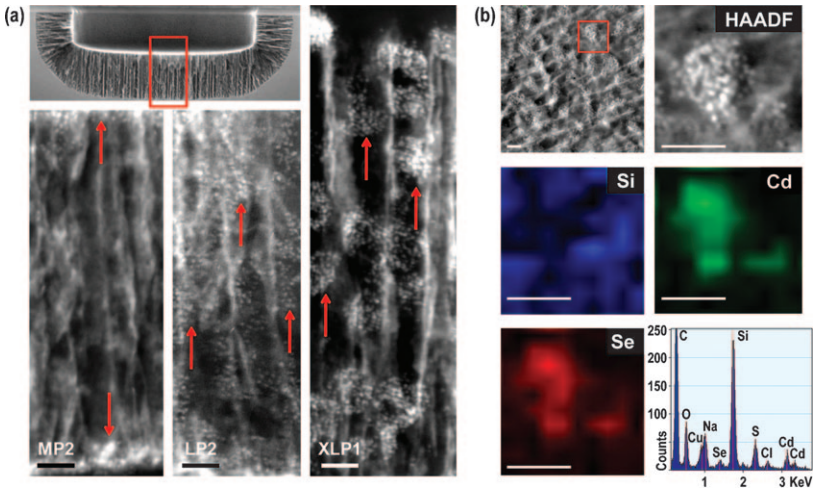

Figure 6. a) HAADF-STEM images of PSPs loaded with 15–20 nm Q-dots. The top SEM image indicates the region analyzed by STEM-HAADF highlighted by a red box. From left to right, 15.2 nm pore MP2 PSP, 26.3 nm pore LP2 PSP, and 51.3 nm pore XLP1 PSP. Arrows indicate Q-dots. b) STEM-EDX mapping analysis. From left to right, top to bottom: HAADF-STEM image of the region of interest, the red box indicating the region analyzed by mapping EDX; HAADF-STEM image of the analyzed region; EDX intensity map for Si; EDX intensity map for Cd; EDX intensity map for Se; typical STEM-EDX spectrum in the region of interest. All scale bars: 50 nm.

diameter) as electron-dense spots of approximately 5 nm diameter within the Si matrix. Q-dots accumulated on the external surfaces of MPs (and SPs, data not shown) but did not penetrate into the porous matrix due to size exclusion (Figure 6a). Q-dots distributed uniformly, in a close-packed structure, within the porous matrix of LPs whereas they formed aggregate structures within the matrix of XLPs (Figure 6a). While the electrostatic interaction between Q-dots and the PSP played an important role in the adhesion of the Q-dots on the surface of the PSP, the ability of the Q-dots to access or not the MP porous matrix was explained by size exclusion. Similarly, the formation of Q-dot aggregates observed within the matrix of XLPs suggested an important role of the electrostatic interaction between the Q-dots and the pore walls. Furthermore, the interaction between the carboxyl and amine groups provided a stable bond that allowed loading and retention of the Q-dots within the porous matrix. Upon exposure of the PSP to physiological conditions the biodegradation of the PSP walls will determine the shedding of the silane, thus allowing the free diffusion of Q-dots from the matrix that results in their sustained release.[9]

The mapping EDX analysis of the porous matrix of an XLP1 (Figure 6b) showed co-localization of Cd and Se signals with the electron-dense clusters detected by HAADF-STEM, which provided elemental analysis confirmation of Q-dot loading. Furthermore, we employed HAADF-STEM tomographic imaging[29,30] of the porous matrix of an XLP1 (Supporting Information, Videos 1 and 2) to confirm the spatial localization of the Q-dots within the porous matrix.

Conclusions

We have demonstrated the ability to microfabricate PSPs with tailored features at the nanoscale. We controlled with submicrometer precision the size (from 0.97 to 3.2 μm) and shape (rounded square) of the nucleation side of the PSP through the size and shape of the photolithographic pattern. We controlled the PSP profile using different silicon-etch protocols, which resulted in aspect ratios ranging from 1.8 to 5.3 and overall shapes ranging from discoidal to hemispherical to tubular. Control of the PSP aspect ratio can be exploited to affect their biodistribution following intravenous injection,[31] while size and shape control are predicted to affect cell uptake mechanisms and kinetics.[32] Furthermore, we demonstrated the ability to tailor the porous structure of a PSP to control the loading of second-stage NPs. We proved the ability to tailor pore size (from 5 to over 50 nm) and porosity (from 47 to over 80%) while preserving the mechanical stability and integrity of the PSP. We described the effect of pore size on the loading of second-stage NPs and identified the existence of an optimal pore size for their uniform, close-packed loading. In conclusion, we have demonstrated the ability to tune particles and pore features over the range that allows potential tailoring of PSPs as delivery agents for combinations of specific biomedically relevant NPs. The tools and protocols provided by this study constitute the foundation for the successful development and use of PSPs for the delivery of NPs in biomedical applications.

Experimental Section

Sacrificial Layer Patterning: In a class 100 clean room, a uniform masking layer of silicon-rich silicon nitride was deposited in a low-pressure chemical vapor deposition furnace (90 nm, 835 °C, 300 mTorr, SiH_2Cl_2/NH_3 80:20%, 25 min) on a heavily doped 4-inch p++-type (100) wafer with resistivity less than 0.005 Ω cm (Silicon Quest, Inc., Santa Clara, CA). Circles 2 or 1 μm in diameter with 2 and 1 μm half-pitch, respectively, were patterned on the nitride film by means of contact photolithography (AZ-5209 photoresist, EVG-620 aligner, 40 J dose). The wafer was reactive-ion etched in pure CF_4 plasma (Plasmatherm 790 series, 15 sccm CF_4, 200 mTorr, 250 W radio-frequency (RF) power, 2 min) to transfer the pattern into the nitride layer on the front side and avoid overetching into the silicon.

Silicon Etch: Following patterning of the sacrificial layer, a trench was formed in the silicon wafer by a second dry or wet etch step. The etch was chosen as a combination of the following processes depending on the desired final shape: SF_6 (Oxford Plasmalab 80 plus, 10 sccm SF_6, 100 mTorr, 300 W RF power), CF_4 (Plasmatherm 790 series, 15 sccm CF_4, 200 mTorr, 250 W RF power), HBr (Plasma-

therm 790 series, 4 sccm Cl_2, 25.4 sccm HBr, 150 mTorr, 250 W RF power) and buffered oxide etch (BoE).

Electrochemical Etch: The rear side of the wafer was exposed to CF_4 RIE (Plasmatherm 790 series, 15 sccm CF_4, 200 mTorr, 250 W RF power, 2.5 min) to remove the nitride film, and coated with 200 nm of sputtered aluminum (Varian Sputter) to provide a uniform rear-side electrical contact. A custom-made poly(tetrafluoroethylene) electrochemical etch cell with an aluminum-foil anode and a platinum-mesh cathode was used for anodic electrochemical etching. The anode was contacted to the aluminum-coated rear side of the wafer and not exposed to the etchant solution, while the cathode faced the front side of the patterned wafer at a fixed distance. The wafer was electrochemically etched for the time necessary to obtain the desired PSP thickness by applying the current density and HF/ethanol ratio described in Figure 4b. Following formation of the PSP, a high current density was applied to form a high-porosity layer at the PSP/wafer interface (release layer).

PSP Release: The silicon nitride masking layer was stripped in 49% HF for 30 min. The wafer was rinsed and spin-dried, then placed in a glass crystallization dish filled with IPA (40 mL) and sonicated for 1 min to detach the PSPs from the bulk wafer. Finally, the release suspension was transferred to a 50 mL low-retention tube and stored in a controlled-temperature environment at 20 °C.

Nitrogen Absorption/Desorption: The surface area and pore size of the PSPs were measured using N_2 adsorption–desorption isotherms on a Quantachrome Autosorb-3B surface analyzer. To prepare the sample, PSPs (10 mg) suspended in IPA from ten independent processes were mixed and centrifuged, and the supernatant was removed leaving about 3 mL PSPs–IPA suspension. The suspension was transferred to a sample cell in a vacuum oven at 80 °C to evaporate the solvent. The sample was degassed at 200 °C for 12 h, and the N_2 adsorption–desorption isotherm was measured at 77 K over the relative pressure (P/P_0) range of 0.015–0.995. Nanopore size distributions and porosities were calculated from the desorption branch of the isotherms using the BJH model.

Removal of the Nucleation Layer: Following the electrochemical etch, but preceding the removal of the sacrificial layer, the patterned substrate containing the PSPs was dry etched in CF_4 plasma (Plasmatherm 790 series, 10 sccm CF_4, 25 mTorr, 200 W RF power, 18 s).

Loading: SPs, MPs, LPs, and XLPs were oxidized and conjugated with APTES, which resulted in a positively charged amine-terminated PSP surface. A tris(hydroxymethyl)aminomethane-HCl buffered suspension (100 mL, pH 7.3) of PSPs and 15-nm-diameter carboxyl-functionalized CdSe Q-dots (1 mM, Qdot 565 ITK Invitrogen, Carlsbad, CA) was incubated on a rotating wheel for 15 min. The suspension was centrifuged for 10 min at 16000 rpm in a fixed-angle tabletop microcentrifuge.

TEM Sample Preparation: The supernatant was removed from the loaded PSP suspension, and the pellet was resuspended in deionized water (20 mL) and brought to 40 °C in a water bath. Low-melt 4% agarose solution (100 mL) kept at 60 °C was added to the suspension, which was immediately centrifuged for 20 min at 16000 rpm in a fixed-angle tabletop microcentrifuge. The resulting PSP-rich gel was diced into 1 mm^3 cubes and dehydrated with subsequent rinses in 30, 70, and 100% anhydrous ethanol followed by 100% acetone. The gel cubes were transferred to a size 3 embedding capsule and Spurr's resin was added. The capsule was centrifuged for 20 min at 16000 rpm in a fixed-angle tabletop microcentrifuge. The PSP-rich resin was fully cured in an oven at 60 °C for 12 h. Ultrathin slices (100 nm) of PSP-rich resin were microtomed in a Leica UCT apparatus and collected on a 400 mesh Cu TEM grid.

TEM/EDX Analysis: HAADF-STEM analysis and mapping EDX were performed with an FEI Tecnai G2 F20 X-TWIN TEM instrument (FEI Company, Hillsboro, OR) operating at 200 kV with nanoprobe spot 7. EDX analysis was performed with 8000 ms dwell time and 12° tilt.

TEM Tomography: HAADF-STEM tilt series were acquired automatically on an FEI Tecnai F20 S-TWIN TEM instrument operating at 200 kV using the FEI XPlore3D 2.0 tomography suite. The STEM images were collected over an angular range of ±65° in 2° steps below 50° and 1° steps above 50°. The STEM probe size was 0.19 nm. The reconstructions of the tilt series were calculated with an FEI Inspect 3D Express tomography pack using a weighted back-projection (WBP) method and the visualization was carried out using the FEI Resolve RT/Amira software.

Acknowledgements

We thank the Center for Nano and Molecular Science, the Institute for Cellular and Molecular Biology, and the Microelectronics Research Center at the University of Texas at Austin for use of instrumentation and facilities. We thank Dwight Romanovicz for help in experimental design and Matthew Landry for excellent graphical support. We thank Michael Strauss, Pal Ove Pedersen, Brandon Van Leer, and all the team at the North America Nanoport application team of FEI Company (Hillsboro, OR) for providing the facilities and characterization work. These studies were supported by the following grants: State of Texas's Emerging Technology Fund, NASA (NNJ06HE06A), DoD (W81XWH-07-2-0101), and NIH (R01CA128797). The authors would like to recognize the contributions and support from the Alliance for NanoHealth (ANH). Commercialization rights on intellectual property presented in this paper have been acquired by Leonardo Biosystems Inc. M.F. is the founding scientist of Leonardo Biosystems; E.T. and X.L. are stockholders of Leonardo Biosystems.

Keywords: drug delivery · electron microscopy · mesoporous materials · nanoparticles · silicon

[1] L. T. Canham, *Adv. Mater.* **1995**, *7*, 1033 – 1037.
[2] S. H. C. Anderson, H. Elliott, D. J. Wallis, L. T. Canham, J. J. Powell, *Phys. Status Solidi A* **2003**, *197*, 331 – 335.
[3] F. J. Martin, K. Melnik, T. West, J. Shapiro, M. Cohen, A. A. Boiarski, M. Ferrari, *Drugs R&D* **2005**, *6*, 71 – 81.
[4] S. P. Low, K. A. Williams, L. T. Canham, N. H. Voelcker, *Biomaterials* **2006**, *27*, 4538 – 4546.
[5] V. Chin, B. E. Collins, M. J. Sailor, S. N. Bhatia, *Adv. Mater.* **2001**, *13*, 1877 – 1880.
[6] S. C. Bayliss, R. Heald, D. I. Fletcher, L. D. Buckberry, *Adv. Mater.* **1999**, *11*, 318 – 321.
[7] A. S. W. Goh, A. Y. F. Chung, R. H. G. Lo, T. N. Lau, S. W. K. Yu, M. Chng, S. Satchithanantham, S. L. E. Loong, D. C. E. Ng, B. C. Lim, S. Connor, P. K. H. Chow, *Int. J. Radiat. Oncol. Biol. Phys.* **2007**, *67*, 786 – 792.
[8] L. Canham, M. Stewart, J. Buriak, C. Reeves, M. Anderson, E. Squire, P. Allcock, P. Snow, *Phys. Status Solidi A* **2000**, *182*, 521 – 525.
[9] E. Tasciotti, X. Liu, R. Bhavane, K. Plant, A. D. Leonard, B. K. Price, M. M. C. Cheng, P. Decuzzi, J. M. Tour, F. Robertson, *Nat. Nanotechnol.* **2008**, *3*, 151 – 157.

[10] J. Salonen, L. Laitinen, A. M. Kaukonen, J. Tuura, M. Björkqvist, T. Heikkilä, K. Vähä-Heikkilä, J. Hirvonen, V. P. Lehto, *J. Controlled Release* **2005**, *108*, 362 – 374.
[11] W. Sun, J. E. Puzas, T. J. Sheu, P. M. Fauchet, *Phys. Status Solidi A* **2007**, *204*, 1429 – 1433.
[12] Y. Khung, S. D. Graney, N. H. Voelcker, *Biotechnol. Prog.* **2006**, *22*, 1388 – 1393.
[13] C. A. Prestidge, T. J. Barnes, C. Lau, C. Barnett, A. Loni, L. T. Canham, *Expert Opin. Drug Delivery* **2007**, *4*, 101 – 110.
[14] M. Ferrari, *Nat. Rev. Cancer* **2005**, *5*, 161 – 171.
[15] R. E. Serda, J. Gu, R. C. Bhavane, X. Liu, C. Chiappini, P. Decuzzi, M. Ferrari, *Biomaterials* **2009**, *30*, 2440 – 2448.
[16] A. G. Cuenca, H. Jiang, S. N. Hochwald, M. Delano, W. G. Cance, S. R. Grobmyer, *Cancer* **2006**, *107*, 459 – 466.
[17] M. V. Yezhelyev, X. Gao, Y. Xing, A. Al-Hajj, S. Nie, R. M. O'Regan, *Lancet Oncol.* **2006**, *7*, 657 – 667.
[18] L. Brannon-Peppas, J. O. Blanchette, *Adv. Drug Delivery Rev.* **2004**, *56*, 1649 – 1659.
[19] P. Decuzzi, M. Ferrari, *Biomaterials* **2007**, *28*, 2915 – 2922.
[20] J. P. Rolland, B. W. Maynor, L. E. Euliss, A. E. Exner, G. M. Denison, J. M. DeSimone, *J. Am. Chem. Soc.* **2005**, *127*, 10096 – 10100.
[21] F. Gentile, C. Chiappini, D. Fine, R. C. Bhavane, M. S. Peluccio, M. M. Cheng, X. Liu, M. Ferrari, P. Decuzzi, *J. Biomech.* **2008**, *41*, 2312 – 2318.
[22] P. Decuzzi, M. Ferrari, *Biomaterials* **2008**, *29*, 377 – 384.
[23] F. Cunin, T. A. Schmedake, J. R. Link, Y. Y. Li, J. Koh, S. N. Bhatia, M. J. Sailor, *Nat. Mater.* **2002**, *1*, 39 – 41.
[24] M. H. Cohen, K. Melnik, A. A. Boiarski, M. Ferrari, F. J. Martin, *Biomed. Microdevices* **2003**, *5*, 253 – 259.
[25] J. R. Dorvee, M. J. Sailor, G. M. Miskelly, *Dalton Trans.* **2008**, 721 – 730.
[26] L. Cheng, E. Anglin, F. Cunin, D. Kim, M. J. Sailor, I. Falkenstein, A. Tammewar, W. R. Freeman, *Br. J. Ophthalmol.* **2008**, *92*, 705 – 711.
[27] R. Herino in *The Properties of Porous Silicon* (Ed.: L. T. Canham), INSPEC-IEE, London, **1997**, pp. 89 – 96.
[28] X. G. Zhang, *J. Electrochem. Soc.* **2004**, *151*, C69 – C80.
[29] C. Kübel, A. Voigt, R. Schoenmakers, M. Otten, D. Su, T. Lee, S. Carlsson, J. Bradley, *Microsc. Microanal.* **2005**, *11*, 378 – 400.
[30] L. F. Drummy, Y. C. Wang, R. Schoenmakers, K. May, M. Jackson, H. Koerner, B. L. Farmer, D. Mauryama, R. A. Vaia, *Macromolecules* **2008**, *41*, 2135 – 2143.
[31] P. Decuzzi, R. Pasqualini, W. Arap, M. Ferrari, *Pharm. Res.* **2009**, *26*, 235 – 243.
[32] S. E. Gratton, P. A. Ropp, P. D. Pohlhaus, J. C. Luft, V. J. Madden, M. E. Napier, J. M. DeSimone, *Proc. Natl. Acad. Sci. USA* **2008**, *105*, 11613 – 11618.

Received: November 23, 2009
Published online on February 16, 2010

